

Linear and fractal diffusion coefficients in a family of one-dimensional chaotic maps

This article has been downloaded from IOPscience. Please scroll down to see the full text article.

2011 Nonlinearity 24 227

(<http://iopscience.iop.org/0951-7715/24/1/011>)

View [the table of contents for this issue](#), or go to the [journal homepage](#) for more

Download details:

IP Address: 94.1.46.86

The article was downloaded on 10/12/2010 at 11:35

Please note that [terms and conditions apply](#).

Linear and fractal diffusion coefficients in a family of one-dimensional chaotic maps

Georgie Knight and Rainer Klages

School of Mathematical Sciences, Queen Mary University of London, Mile End Road,
London E1 4NS, UK

Received 20 July 2010, in final form 26 October 2010

Published 9 December 2010

Online at stacks.iop.org/Non/24/227

Recommended by C P Dettmann

Abstract

We analyse deterministic diffusion in a simple, one-dimensional setting consisting of a family of four parameter dependent, chaotic maps defined over the real line. When iterated under these maps, a probability density function spreads out and one can define a diffusion coefficient. We look at how the diffusion coefficient varies across the family of maps and under parameter variation. Using a technique by which Taylor–Green–Kubo formulae are evaluated in terms of generalized Takagi functions, we derive exact, fully analytical expressions for the diffusion coefficients. Typically, for simple maps these quantities are fractal functions of control parameters. However, our family of four maps exhibits both fractal and linear behaviour. We explain these different structures by looking at the topology of the Markov partitions and the ergodic properties of the maps.

1. Introduction

One of the most prominent problems in statistical physics and dynamical systems theory is to understand nonequilibrium transport from first principles, that is, starting from the nonlinear equations of motion of many-particle systems [1–3]. Such a theory aims at explaining the origin of macroscopic transport in terms of the chaotic and fractal properties of the underlying microscopic deterministic dynamics. Unfortunately, physical many-particle systems are typically way too complex to allow for exact analytical solutions of this problem. A common strategy is therefore to first study solvable toy models, such as deterministic random walks defined by one-dimensional chaotic maps [4–6], before applying the knowledge gained to more difficult dynamics.

It came as a surprise when the diffusion coefficient in a simple piecewise linear model of this type was found to be a fractal function of a control parameter [7]. That this result was not an artefact of the model used was confirmed by studying other transport processes,

such as biased diffusion [8] and reaction-diffusion [9] in other (nonlinear) maps [10, 11] and in physically more realistic systems like periodic particle billiards [1], which in turn can be linked to experiments [12]; see [3] for a review and further references. Unfortunately, even for the simplest piecewise linear deterministic models exact solutions for transport coefficients are rare [2]: for specific values of control parameters analytical results are available by cycle expansion techniques [10] or by first passage methods [13, 14]. Numerical extensions of these methods include stability ordering of periodic orbits [15] and transition matrix methods [7, 9, 13, 14]. As methods yielding exact formulae for fractal transport coefficients, we know only of the twisted eigenstate method [8] and a dynamical zeta function technique [16].

In order to better understand existence and properties of fractal transport coefficients in chaotic dynamical systems, it is vital to develop both more powerful tools for calculating these quantities, and to enlarge the set of systems studied. Correspondingly, the novelty of this paper is two-fold: we introduce a new family of deterministically diffusive models which, to our knowledge, defines the simplest class of systems exhibiting fractal diffusion coefficients. We then calculate these quantities by a method based on the Taylor–Green–Kubo formula [1–3] in combination with generalized Takagi functions [9, 13]. This approach is for the first time explored analytically to its full power. Our main results are exact analytic expressions for the parameter dependent diffusion coefficients of the whole family of maps and the discovery that there is a mixture of linearity and fractality in the diffusion coefficients. The linearity is non-trivial, because in the regions of linearity the maps are either non-ergodic or topologically unstable. The latter property typically generates fractal parameter dependences, however, our method reveals a subtle mechanism of ‘*dominating branches*’, which can stabilize diffusion coefficients under parameter variation in maps whose microscopic symmetry is broken. We emphasize that the term ‘*linear behaviour*’ used in our paper is not to be confused with that used in irreversible thermodynamics, where it refers to the linear response of fluxes with respect to external forces.

Our paper is organized as follows: in section 2 we introduce the family of maps that are under scrutiny before briefly describing the method we use to obtain the parameter dependent diffusion coefficients in section 3. We also define functional recursive relations for the interesting fractal Takagi functions that we meet. In section 4 we analyse the structure of the diffusion coefficients and explain the features that we observe. Most importantly, we explain why we get a mixture of fractality and linearity. We then employ a method based on the Markov partitions of the maps to pinpoint exactly where the local extrema will be in these fractal diffusion coefficients [7, 13, 14]. In addition we explore the fact that in certain parameter regions the diffusion coefficients are very stable to dramatic changes in the microscopic dynamics of the maps, this property being interestingly opposed to the fact that the diffusion coefficients are extremely sensitive to parameter variation in other areas of the parameter space. Section 5 forms a conclusion.

2. The family of maps

In this section the family of maps and how they are constructed will be introduced.

For $h \geq 0$ let $M_h(x) : [0, 1] \rightarrow \mathbb{R}$ be a parameter dependent variant of the well known Bernoulli shift map. The parameter lifts the first branch, and lowers the second branch, i.e.

$$M_h(x) = \begin{cases} 2x + h & 0 \leq x < \frac{1}{2} \\ 2x - 1 - h & \frac{1}{2} \leq x < 1. \end{cases} \quad (1)$$

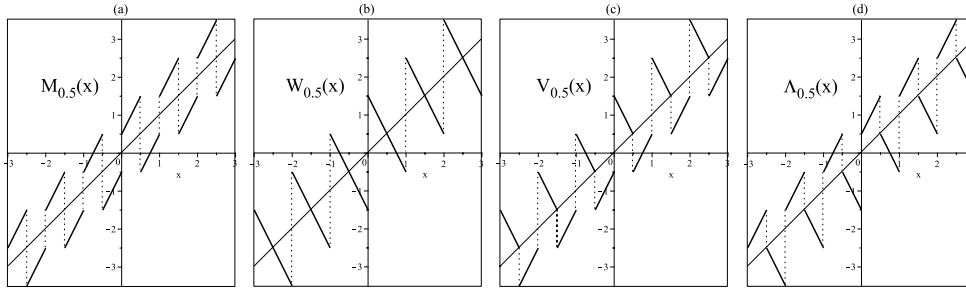


Figure 1. *The family of maps.* In this figure, a section of each of the four maps under scrutiny is illustrated at a parameter value of $h = 0.5$: in (a) the lifted Bernoulli shift, so-called because the Bernoulli shift is recovered when $h = 0$ on the unit interval; in (b) the lifted negative Bernoulli shift, so-called because a version of the Bernoulli shift with a negative gradient is recovered when $h = 0$; in (c) the lifted V map, so-called because a V map is recovered when $h = 0$; in (d) the lifted tent map, so-called because a tent map is recovered when $h = 0$.

In order to create an extended system for diffusion, we define $M_h(x) : \mathbb{R} \rightarrow \mathbb{R}$ by periodically copying equation (1), with a lift of degree one such that

$$M_h(x + n) = M_h(x) + n, \quad n \in \mathbb{Z}. \tag{2}$$

The map described above and its diffusion coefficient were first studied in [9] using a different method. We call it the lifted Bernoulli shift map. This process of copying a map with a lift of degree one is a common way to create a diffusive map [4–6]. The use of the lift parameter h ensures that the invariant probability density function (p.d.f) $\rho^*(x)$ remains a constant function throughout the entire parameter range. This profoundly simplifies the derivation of the diffusion coefficient, as an invariant p.d.f is an essential ingredient in the Taylor–Green–Kubo formula that is used to derive the diffusion coefficient [2, 13].

The remaining members of the family are created by changing the sign of the gradient in equation (1). Let $W_h(x) : [0, 1] \rightarrow \mathbb{R}$

$$W_h(x) = \begin{cases} -2x + h + 1 & 0 \leq x < \frac{1}{2} \\ -2x + 2 - h & \frac{1}{2} \leq x < 1, \end{cases} \tag{3}$$

which we call the lifted negative Bernoulli shift map. Let $V_h(x) : [0, 1] \rightarrow \mathbb{R}$

$$V_h(x) = \begin{cases} -2x + 1 + h & 0 \leq x < \frac{1}{2} \\ 2x - 1 - h & \frac{1}{2} \leq x < 1, \end{cases} \tag{4}$$

which we call the lifted V map. Let $\Lambda_h(x) : [0, 1] \rightarrow \mathbb{R}$

$$\Lambda_h(x) = \begin{cases} 2x + h & 0 \leq x < \frac{1}{2} \\ -2x + 2 - h & \frac{1}{2} \leq x < 1, \end{cases} \tag{5}$$

which we call the lifted tent map. Again we apply the lift of degree one condition of equation (2) to equations (3), (4) and (5) to create spatially extended systems defined over the real line. See figure 1 for an illustration.

3. Deriving the diffusion coefficient

The diffusion coefficient D as a function of h for the four maps is given by the Taylor–Green–Kubo formula [1–3]

$$D(h) = \lim_{n \rightarrow \infty} \left(\int_0^1 v_0(x) \sum_{k=0}^n v_k(x) \rho^*(x) \, dx \right) - \frac{1}{2} \int_0^1 v_0(x)^2 \rho^*(x) \, dx, \quad (6)$$

which simplifies with $\rho^*(x) = 1$ for our maps, and $v_k(x) : \mathbb{R} \rightarrow \mathbb{Z}$,

$$v_k(x) = \lfloor x_{k+1} \rfloor - \lfloor x_k \rfloor, \quad (7)$$

gives the integer value of the displacement of a point x at the k th iteration. The second integral of equation (6) is simple enough to solve; however, the first integral is more involved, so we use a recursive method. We first define a cumulative ‘jump function’ $J_M^n(x) : [0, 1] \rightarrow \mathbb{R}$,

$$\begin{aligned} J_M^n(x) &= \sum_{k=0}^n v_k(x) \\ &= v_0(x) + J_M^{n-1}(\tilde{M}_h(x)). \end{aligned} \quad (8)$$

which gives the integer displacement of a point x after n iterations. The subscript M tells us we are considering the jump function for the lifted Bernoulli shift map $M_h(x)$, and $\tilde{M}_h(x)$ is equation (1) taken modulo 1. We then define an integral over equation (8), $T_M(x) : [0, 1] \rightarrow \mathbb{R}$,

$$T_M(x) = \lim_{n \rightarrow \infty} T_M^n(x) = \lim_{n \rightarrow \infty} \int_0^x J_M^n(y) \, dy. \quad (9)$$

Equation (9) defines the ‘generalized Takagi functions’ discussed in [13]. Due to the chaotic nature of the maps, and in particular, the sensitive dependence on initial conditions, the jump function behaves very erratically for large n . This is reflected in $T_M(x)$ which becomes fractal in the limit as $n \rightarrow \infty$. We solve equation (9) recursively using equation (8) combined with the property that $T^n(0) = T^n(1) = 0$ and that these generalized Takagi functions are continuous [2, 13]. The recursion relation for $T_M(x)$ is given by

$$T_M(x) = \begin{cases} \frac{1}{2} T_M(2x + \hat{h}) + \lfloor h \rfloor x - \frac{1}{2} T_M(\hat{h}) & 0 \leq x < \frac{1 - \hat{h}}{2} \\ \frac{1}{2} T_M(2x + \hat{h} - 1) + \lceil h \rceil x + \frac{\hat{h} - 1}{2} - \frac{1}{2} T_M(\hat{h}) & \frac{1 - \hat{h}}{2} \leq x < \frac{1}{2} \\ \frac{1}{2} T_M(2x - \hat{h}) + \frac{1 + \hat{h}}{2} - \lceil h \rceil x - \frac{1}{2} T_M(\hat{h}) & \frac{1}{2} \leq x < \frac{1 + \hat{h}}{2} \\ \frac{1}{2} T_M(2x - 1 - \hat{h}) - \lfloor h \rfloor x + \lfloor h \rfloor - \frac{1}{2} T_M(\hat{h}) & \frac{1 + \hat{h}}{2} \leq x \leq 1, \end{cases} \quad (10)$$

where we have taken the limit $n \rightarrow \infty$, and \hat{h} is defined as

$$\hat{h} = \begin{cases} 1 & h \in \mathbb{Z} \\ h \bmod 1 & \text{otherwise.} \end{cases} \quad (11)$$

Equation (11) is simply a corrective function that ensures equation (10) is correct at the points of discontinuity. An illustration of equation (10) with $h = 1$ can be seen in figure 2(a). For details about the evaluation of this Takagi function and the ones for the other three maps of our family cf [20].

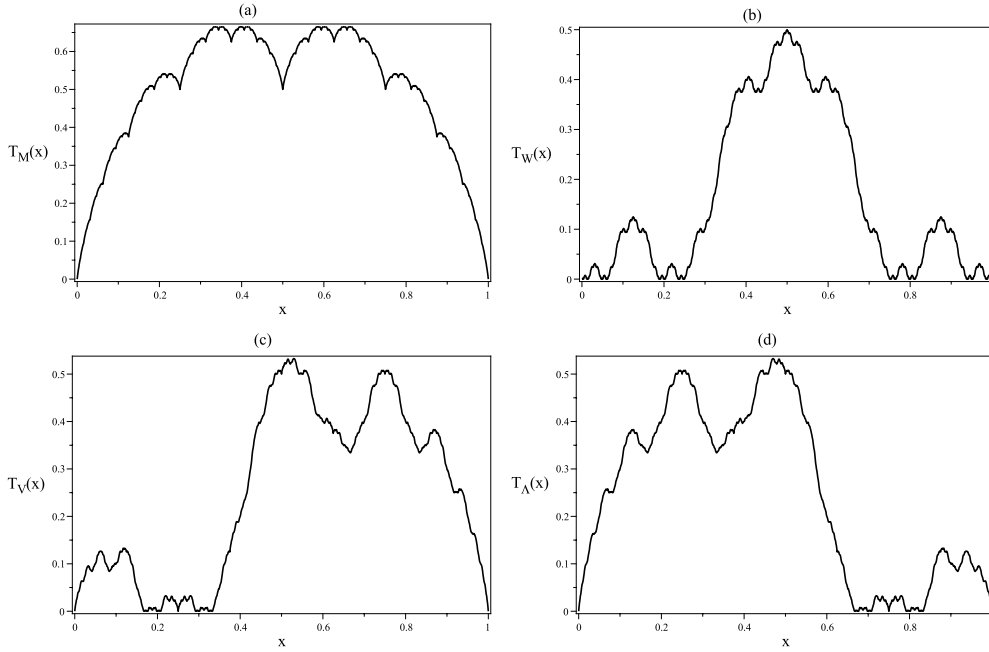


Figure 2. *The Takagi functions.* In this figure, the Takagi functions are shown for the four maps at a parameter value of $h = 1$: in (a) the lifted Bernoulli shift, which you may recognize as the famous Takagi function; in (b) the negative Bernoulli shift; in (c) the lifted V map; in (d) the lifted tent map. Note the self similarity and ‘fractal’ structure. Note also the asymmetry in (c) and (d) compared with (a) and (b). This is due to the asymmetry in the evolution of the p.d.f for these maps. Also portrayed here is that $T_V(x) = T_\Lambda(1 - x)$.

We now have the ingredients that we need to derive the parameter dependent diffusion coefficient. We first apply equation (8) to the Taylor–Green–Kubo formula to obtain

$$\begin{aligned}
 D_M(h) &= \lim_{n \rightarrow \infty} \left(\int_0^1 v_0(x) J_M^n(x) dx \right) - \frac{1}{2} \int_0^1 v_0^2(x) dx \\
 &= \lim_{n \rightarrow \infty} \int_0^{\frac{1-\hat{h}}{2}} \lceil h \rceil J_M^n(x) dx + \int_{\frac{1-\hat{h}}{2}}^{\frac{1}{2}} \lceil h \rceil J_M^n(x) dx - \int_{\frac{1}{2}}^{\frac{1+\hat{h}}{2}} \lceil h \rceil J_M^n(x) dx \\
 &\quad - \int_{\frac{1+\hat{h}}{2}}^1 \lceil h \rceil J_M^n(x) dx - \frac{1}{2} \left(\int_0^{\frac{1-\hat{h}}{2}} \lceil h \rceil^2 + \int_{\frac{1-\hat{h}}{2}}^{\frac{1}{2}} \lceil h \rceil^2 + \int_{\frac{1}{2}}^{\frac{1+\hat{h}}{2}} \lceil h \rceil^2 + \int_{\frac{1+\hat{h}}{2}}^1 \lceil h \rceil^2 \right). \quad (12)
 \end{aligned}$$

Evaluating the integrals, simplifying by using equation (10) and gathering relevant terms we obtain

$$D_M(h) = \frac{\lceil h \rceil^2}{2} + \left(\frac{1 - \hat{h}}{2} \right) (1 - 2\lceil h \rceil) + T_M(\hat{h}). \quad (13)$$

Equation (13) is an exact analytic expression for the parameter dependent diffusion coefficient of the lifted Bernoulli shift map. The first two terms in this equation form a piecewise linear function that is equal to $h^2/2$ for large h , which defines the asymptotic growth of the diffusion coefficient in this parameter regime. Interestingly, our shifted map thus belongs to a different universality class compared with the maps studied in [13, 17] where the gradient was varied as

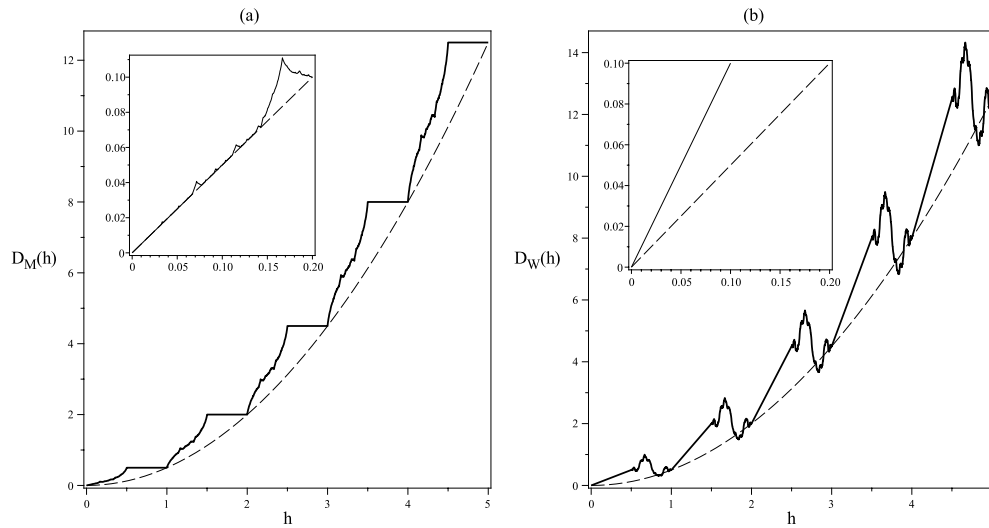


Figure 3. Large scale structure and asymptotic behaviour. In this figure, the diffusion coefficients for the lifted Bernoulli shift (a) and the lifted negative Bernoulli shift (b) are illustrated. Also included in both is $f(h) = h^2/2$ to show how the function grows for large h . Note the periodicity of the fine scale structure. Inset in both is an illustration of the asymptotic behaviour as $h \rightarrow 0$. The dashed lines are $h/2$ to show the different behaviour.

a control parameter yielding a coefficient of $1/6$ for the quadratic scaling in this regime. The last term $T_M(\hat{h})$ in equation (13) tells us about the fine structure of $D_M(h)$, which is periodic modulo 1 as it is a function of \hat{h} , see figure 3 for an illustration. For small h we get a different region of asymptotic behaviour where the diffusion coefficient is given by

$$D_M(h) = \frac{h}{2} + T_M(h) \quad 0 \leq h \leq 1. \quad (14)$$

In this regime equation (10) yields $T_M(h) = \frac{1}{3}T_M(3h)$, that is, if we make h smaller by a factor of 3 the deviation from $h/2$ in the diffusion coefficient is also reduced by a factor of 3. This explains why the fine structure that we observe in the inset of figure 3(a) becomes smaller and smaller in the limit of $h \rightarrow 0$. The diffusion coefficient thus behaves asymptotically like $h/2$ corresponding to the simple random walk result for diffusion in this map for small parameter values. In other words, higher order correlations of our system are negligible as $h \rightarrow 0$, in agreement with the findings in [13, 17]. Such a change between two different types of asymptotic random walk behaviour for small and large parameter values was denoted as a crossover in deterministic diffusion [17].

Although the derivation of equation (13) has been presented for the lifted Bernoulli shift, the method is the same for the other three maps [20].

4. The structure of the diffusion coefficients

In this section the parameter dependent diffusion coefficients for the four maps will be shown, and their structure explained.

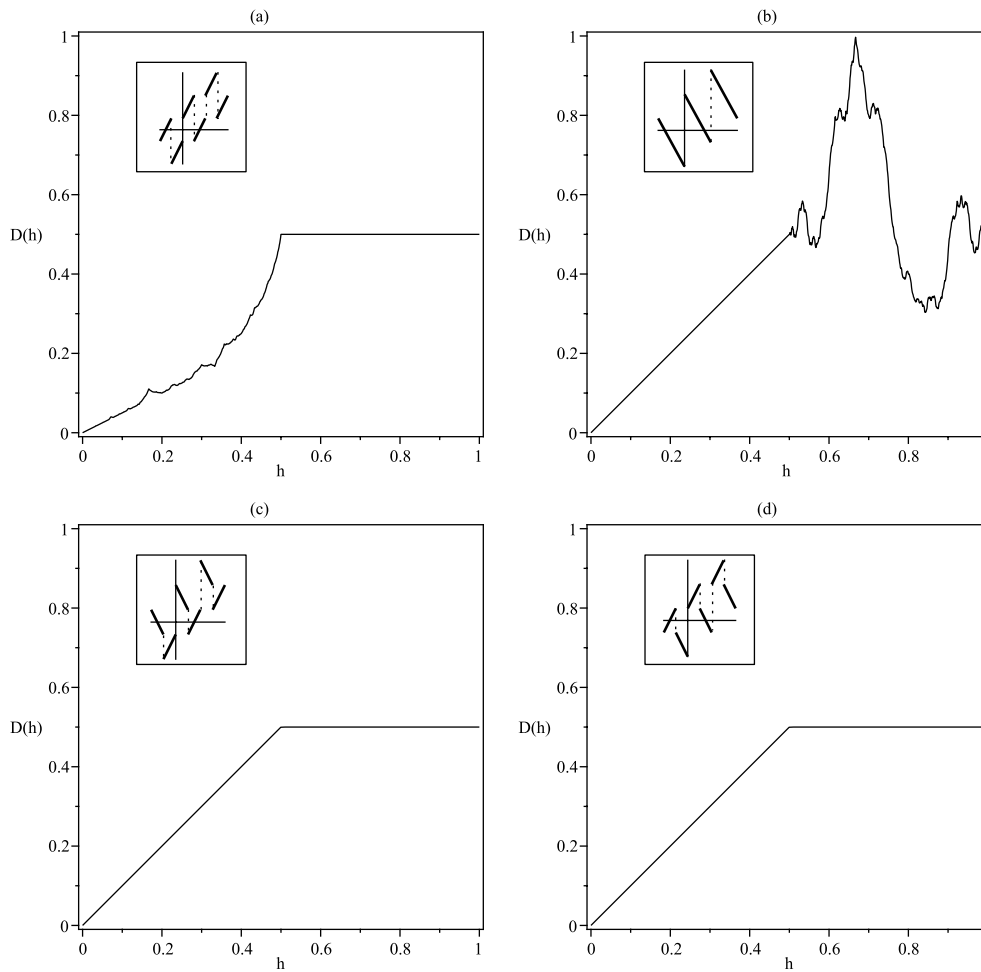


Figure 4. *The diffusion coefficients.* In this figure, the parameter dependent diffusion coefficients are illustrated for (a) the lifted Bernoulli shift; (b) the lifted negative Bernoulli shift; (c) the lifted V map; and (d) the lifted tent map.

4.1. The lifted Bernoulli shift map

Figure 4(a) gives the diffusion coefficient for the lifted Bernoulli shift map. The two striking features are the fractal region when h is between zero and a half, and the linear plateau when h is between a half and one. These regions will be explained in turn.

4.1.1. The fractal region. Firstly, the term ‘*fractal*’ has no strict mathematical definition so we use the term loosely. In particular we use it to refer to the fact that the diffusion coefficient exhibits non-trivial fine scale structure, and regions of scaling and self similarity; for a discussion of this see [18].

The topological instability of the map under parameter variation is reflected in the fractal structure of the diffusion coefficient [3]. So in order to understand the fractality, we need to understand the topological instability. To this end, we take equation (1) modulo 1, and analyse the behaviour of the Markov partitions of the interval map $\tilde{M}_h(x) : [0, 1] \rightarrow [0, 1]$.

The structure of the Markov partitions of $\tilde{M}_h(x)$ varies wildly under parameter variation. The method we employ to understand the Markov partitions involves iterating the critical point $x = \frac{1}{2}$, see [7, 13, 14]. The set of iterates of this point, along with the set of points symmetric about $x = \frac{1}{2}$, will form a set of Markov partition points for the map. Hence we call the orbit of $x = \frac{1}{2}$ a ‘generating orbit’. Furthermore, if the generating orbit is finite for a particular value of h , we obtain a finite Markov partition. We can then use the finite Markov partition to tell us about the diffusive properties of the map and hence the structure of the diffusion coefficient. For this purpose the following proposition is crucial.

Proposition. *The set of values of the parameter h which give a finite Markov partition are dense in the parameter space.*

Proof.

We show that when h is rational, the generating orbit is finite. This is achieved by showing that the denominator of h fixes the number of possible iterates of the generating orbit. Let $h = a/b$ where $a, b \in \mathbb{N}$ and $a \leq b$

$$\begin{aligned}\tilde{M}_{\frac{a}{b}}(0.5) &= 1 - h \\ &= \frac{b - a}{b}.\end{aligned}\tag{15}$$

Clearly, $b - a \in \{0, 1, 2, \dots, b - 1\}$. If $\tilde{M}_{a/b}((b - a)/b)$ is then evaluated, there are four possibilities due to the four branches of $\tilde{M}_h(x)$. It is not hard to show that for all four possibilities

$$\tilde{M}_{\frac{a}{b}}\left(\frac{b - a}{b}\right) = \frac{c}{b}, \quad c \in \{0, 1, 2, \dots, b - 1\}.\tag{16}$$

So for $n = 1$ and $n = 2$

$$\tilde{M}_{\frac{a}{b}}^n(0.5) = \frac{c}{b},\tag{17}$$

with $c \in \{0, 1, 2, \dots, b - 1\}$. Now we assume that

$$\tilde{M}_{\frac{a}{b}}^m(0.5) = \frac{c}{b}\tag{18}$$

for all $m \leq n$, and the result follows by induction that

$$\tilde{M}_{\frac{a}{b}}^n(0.5) = \frac{c}{b}, \quad c \in \{0, 1, 2, \dots, b - 1\} \quad \forall n \in \mathbb{N}.\tag{19}$$

The result in (19) puts a limit on the size of the subset of values that the orbit of $x = 0.5$ can hit at a given rational value of h , this size being equal to $|\{0, \frac{1}{b}, \dots, \frac{b-1}{b}\}| = b$. Hence the orbit must be periodic, i.e.

$$\tilde{M}_h^n(0.5) = 0.5, \quad n \in \mathbb{N},\tag{20}$$

or pre-periodic, i.e. $\exists k > 0$ such that $\forall m \geq k, k, m, n \in \mathbb{N}$,

$$\tilde{M}_h^n(0.5) = \tilde{M}_h^{n+m}(0.5),\tag{21}$$

and the Markov partition of the map must have a finite number of partition points when h is rational. q.e.d

The second important result is that the finite Markov partitions correspond to the local minima and maxima of the diffusion coefficient [7, 13, 14]. If we extend our view back to the full maps, we see that if the generating orbit is periodic then this corresponds to a relatively high rate of diffusion for the parameter value, which is reflected in the diffusion coefficient

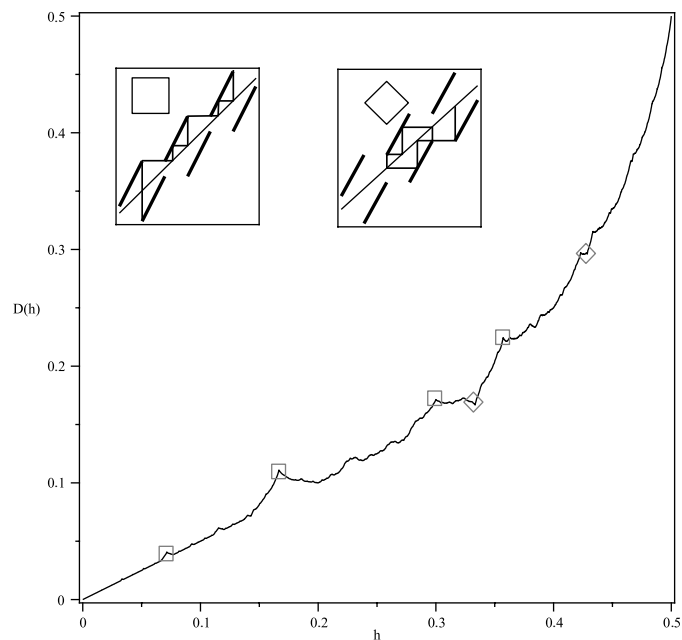


Figure 5. *Pinpointing the local extrema.* In this figure, some of the local extrema have been highlighted. At the points highlighted by squares we see the orbit of 0.5 is iterated to infinity resulting in a local maximum. At the points highlighted by diamonds we see the orbit of 0.5 is in a closed loop resulting in a local minimum.

as a local maximum. In contrast, if the generating orbit is pre-periodic, this corresponds to a relatively low rate of diffusion for the parameter value, which is reflected in the diffusion coefficient as a local minimum. So given that we have a dense set of local maxima and minima, we observe a fractal diffusion coefficient. Furthermore, equation (20) furnishes us with the means of pinpointing the local maxima of the diffusion coefficient. Note that in [13] this technique gave an approximation of where the local extrema were. This model allows us to find them precisely, due to the simplicity of the invariant density. Each n gives us a set of simple linear equations for the variable h , the solutions of which are the local maxima in the diffusion coefficient. In addition, the smaller values of n give the most striking local maxima. One can apply a similar technique to locate the local minima of the graph, see figure 5. However, it is not a case of finding solutions to one simple equation like (20). Rather, there are many ways to define pre-periodic orbits as opposed to defining periodic orbits. In addition, the local minima do not adhere to such a strict ordering that the local maxima do. This is due to the fact that there are two components to a pre-periodic orbit, namely the transient length and the periodic orbit length. In summary, for h between zero and one half, there exists a dense set of points which are either local maxima or local minima. Hence a fractal structure is observed.

4.1.2. The linear region. The second feature of the diffusion coefficient is the linear region where $0.5 \leq h \leq 1$. Not only is it striking because it very abruptly changes from fractal to linear, it is also counter intuitive if we apply a simple random walk approximation to the map. That is, we can obtain a first order approximation of the diffusion coefficient by looking at the measure of the escape region of the map (the area where a point can move from one unit interval to the next) [13, 17]. This region clearly increases linearly with the parameter, so based on a

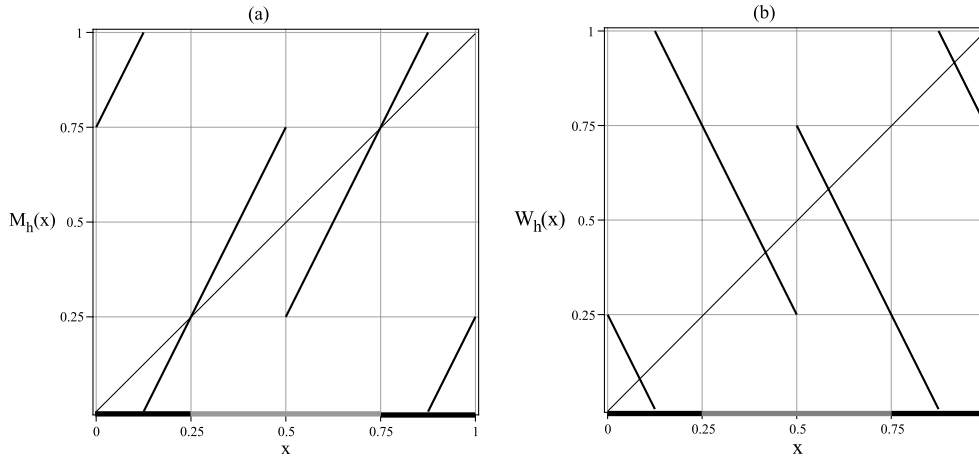


Figure 6. *Non-ergodicity.* In this figure, the nonergodicity of the lifted Bernoulli shift map at $h = 0.75$ is shown in (a), and in the lifted negative Bernoulli shift at $h = 0.25$ in (b). For simplicity the dynamics have been reduced to the maps modulo 1. One can see that the black areas get mapped into themselves as do the grey areas. This splits up the phase space breaking ergodicity.

first order approximation one would expect to see a general increase in the diffusion coefficient as the parameter increases. However, what is observed defies this. We explain this feature by noting that the map is non-ergodic in this region: when the parameter h reaches one half, a fixed point is born in the modulo 1 map. As the parameter increases further, the fixed point bifurcates and the two resulting fixed points split the phase space up into two invariant sets, breaking the ergodicity of the map, see figure 6. Consequently, the invariant density $\rho^*(x)$ can be interpreted as the sum of two invariant densities $\rho_1^*(x)$ and $\rho_2^*(x)$ and the diffusion coefficient can be evaluated as

$$\begin{aligned}
 D_M(h) &= \lim_{n \rightarrow \infty} \frac{1}{2n} \int_0^1 \rho^*(x) (x_n - x_0)^2 dx \\
 &= \lim_{n \rightarrow \infty} \frac{1}{2n} \left(\int_0^1 \rho_1^*(x) (x_n - x_0)^2 dx + \int_0^1 \rho_2^*(x) (x_n - x_0)^2 dx \right). \quad (22)
 \end{aligned}$$

We can then use the Taylor–Green–Kubo formula and derive two separate generalized Takagi functions, in order to evaluate the diffusion coefficient as

$$\begin{aligned}
 D_M(h) &= (1 - h) + (h - \frac{1}{2}) \\
 &= \frac{1}{2}. \quad (23)
 \end{aligned}$$

We see that we have two separate regions of the map whose diffusion coefficients both change smoothly as the parameter varies and complement each other to produce a linear diffusion coefficient.

4.2. The negative Bernoulli shift

Figure 2(b) shows the Takagi function for the lifted negative Bernoulli shift $W_h(x)$ at $h = 1$ and figure 4(b) its diffusion coefficient. Firstly we note how radically different the structure of the diffusion coefficient is from the lifted Bernoulli shift map. In addition, as $h \rightarrow 0$ the diffusion coefficient does not go to $h/2$ by reproducing the random walk solution as in the lifted

Bernoulli shift map. However, as $h \rightarrow \infty$ the diffusion coefficient goes to $h^2/2$ as in the lifted Bernoulli shift. We also observe both a linear and a fractal region. For $0 \leq h \leq \frac{1}{2}$ the diffusion coefficient is a simple linear function equal to h . Again, the explanation for this is that the map is non-ergodic in this parameter range, see figure 6. The phase space is split up into two invariant regions, one of which does not contribute to diffusion as it is a trapping region, the other of which grows linearly with h so we observe a linear, increasing diffusion coefficient. When $\frac{1}{2} \leq h \leq 1$, the map becomes topologically unstable under parameter variation. Similar to the lifted Bernoulli shift map, this instability is reflected in the behaviour of the Markov partitions of (4) taken modulo 1. We have that the finite Markov partitions are dense in the parameter space and that these finite Markov partitions correspond to the local maxima and minima of the diffusion coefficient. Hence we observe a fractal diffusion coefficient.

4.3. The lifted V map

The diffusion coefficient for the lifted V map is given by

$$D_V(h) = \frac{h}{2} + \frac{1}{2}(T_V(h) + T_V(1-h)), \quad 0 \leq h \leq 1, \tag{24}$$

where for $0 \leq h \leq 1$

$$T_V(x) = \begin{cases} x - \frac{1}{2}T_V(-2x+h) + \frac{1}{2}T_V(h) & 0 \leq x < \frac{h}{2} \\ -\frac{1}{2}T_V(-2x+1+h) + \frac{h}{2} + \frac{1}{2}T_V(h) & \frac{h}{2} \leq x < \frac{1}{2} \\ -x + \frac{1}{2}T_V(2x-h) + \frac{h}{2} + \frac{1}{2} - \frac{1}{2}T_V(1-h) & \frac{1}{2} \leq x < \frac{1+h}{2} \\ \frac{1}{2}T_V(2x-1-h) - \frac{1}{2}T_V(1-h) & \frac{1+h}{2} \leq x < 1. \end{cases} \tag{25}$$

For an illustration of the Takagi function defined by this equation see figure 2(c). Instead of evaluating this equation numerically we can use the helpful property that for h less than one half

$$\begin{aligned} T_V(h) &= -\frac{1}{2}T_V(1-h) + \frac{h}{2} + \frac{1}{2}T_V(h) \\ &= -T_V(1-h) + h. \end{aligned} \tag{26}$$

Using equation (26) in equation (24), the diffusion coefficient can be evaluated to

$$\begin{aligned} D_V(h) &= \frac{h}{2} + \frac{1}{2}(-T_V(1-h) + h + T_V(1-h)) \\ &= h. \end{aligned} \tag{27}$$

Furthermore, for h greater than one half

$$\begin{aligned} T_V(h) &= -h + \frac{1}{2}T_V(h) + \frac{h}{2} + \frac{1}{2} - \frac{1}{2}T_V(1-h) \\ &= -T_V(1-h) - h + 1. \end{aligned} \tag{28}$$

Using equation (28) in equation (24), the diffusion coefficient can again be evaluated to

$$\begin{aligned} D_V(h) &= \frac{h}{2} + \frac{1}{2}(-T_V(1-h) - h + 1 + T_V(1-h)) \\ &= \frac{1}{2}. \end{aligned} \tag{29}$$

See figure 4(c) for an illustration.

4.4. The lifted tent map

For the lifted tent map $\Lambda_h(x)$, we cannot perform the same trick with the Takagi functions that we did with the lifted V map in section 4.3. However, we still do not need to resort to numerical computations to see what the diffusion coefficient looks like as we can note that

$$\Lambda_h(x) = -V_h(-x). \quad (30)$$

Equation (30) is important because it serves as a topological conjugacy of the form $f(x) = -x$. By using the Taylor–Green–Kubo formula, equation (6), it was shown in [11] that the diffusion coefficient is preserved by such transformations, hence we observe an identical diffusion coefficient in the two maps, which can be seen in figure 4; see [20] for a simpler version of such a proof.

From what we have learned from the lifted Bernoulli shift map and the lifted negative Bernoulli shift map, we would expect to find non-ergodicity in the lifted tent and lifted V maps. Furthermore we would expect to find it across the entire parameter range given the linear diffusion coefficients. However, there is no obvious non-ergodicity, and although a proof that the maps are ergodic across the entire parameter range remains elusive, we can check for ergodicity at individual values of the parameter by checking the reducibility of the transition matrices [19]. So we can confirm ergodicity for some values of h . Furthermore, the behaviour under parameter variation of the Markov partitions of the maps (4) and (5) taken modulo 1 indicates the presence of topological instability in the parameter space. So, although all the ingredients for a fractal diffusion coefficient are present, we observe a piecewise linear one.

In order to understand the linearity of the diffusion coefficient of the lifted V map, and hence the lifted tent map as well, we first note the similarity of the linear region in the diffusion coefficient of the lifted Bernoulli shift map to the same regions in the diffusion coefficients of the lifted tent and V maps, compare figure 4(a) with (c) and (d). We see an analogous similarity when we compare the diffusion coefficient of the negative Bernoulli shift with that of the lifted tent and V maps, compare figure 4(b) with (c) and (d). This raises the question: why do these maps show the same diffusion coefficients when they exhibit such different microscopic dynamics?

We will explain the linearity of the diffusion coefficients of the lifted tent and lifted V maps by showing why they have the same diffusion coefficients as the two Bernoulli shift maps in the relevant parameter ranges. We will take these ranges in turns, starting with $0.5 \leq h \leq 1$. The diffusion coefficient for the lifted Bernoulli shift map is given by equation (13) which for $h \in [0.5, 1]$ simplifies to

$$D_M(h) = \frac{h}{2} + T_M(h) \quad (31)$$

and can be rewritten as

$$D_M(h) = \frac{h}{2} + \lim_{n \rightarrow \infty} \left(\left(\sum_{k=0}^{n-1} \frac{t_M(h)}{2^{k+1}} \right) + \frac{t_M(h)}{2^n} \right), \quad (32)$$

where $t_M(x) : [0, 1] \rightarrow \mathbb{R}$ is defined as

$$t_M(x) = \int_0^x v_0(y) \, dy, \quad (33)$$

which equals

$$t_M(x) = \begin{cases} 0 & 0 \leq x < \frac{1-h}{2} \\ \frac{h-1}{2} + x & \frac{1-h}{2} \leq x < \frac{1}{2} \\ \frac{h+1}{2} - x & \frac{1}{2} \leq x < \frac{1+h}{2} \\ 0 & \frac{1+h}{2} \leq x \leq 1. \end{cases} \tag{34}$$

A detailed derivation of equation (32) is given in [20], which tells us how the diffusion coefficient converges as $n \rightarrow \infty$. Now, keeping equation (32) in mind, we turn our attention to the lifted V map. The diffusion coefficient for the lifted V map with $h \in [0, 1]$ is given by

$$D_V(h) = \frac{h}{2} + \lim_{n \rightarrow \infty} \left(\frac{1}{2} T_V^{n-1}(h) + \frac{1}{2} T_V^{n-1}(1-h) \right). \tag{35}$$

From equation (25) we can derive the useful recursion relation

$$T_V^n(h) = t_V(h) + \frac{1}{2} T_V^{n-1}(h) - \frac{1}{2} T_V^{n-1}(1-h) \tag{36}$$

where

$$t_V(x) = \begin{cases} x & 0 \leq x < \frac{h}{2} \\ \frac{h}{2} & \frac{h}{2} \leq x < \frac{1}{2} \\ \frac{h+1}{2} - x & \frac{1}{2} \leq x < \frac{1+h}{2} \\ 0 & \frac{1+h}{2} \leq x \leq 1 \end{cases} \quad 0 \leq h \leq 1. \tag{37}$$

If we evaluate equation (36) recursively we get

$$T_V^n(h) = \sum_{k=0}^n \frac{1}{2^k} t_V(h) - \sum_{k=1}^n \frac{1}{2^k} T_V^{n-k}(1-h). \tag{38}$$

Using equation (38) in equation (35) yields

$$D_V(h) = \frac{h}{2} + \lim_{n \rightarrow \infty} \left(\sum_{k=0}^{n-1} \frac{t_V(h)}{2^{k+1}} + \frac{1}{2} \left(T_V^{n-1}(1-h) - \sum_{k=1}^{n-1} \frac{1}{2^k} T_V^{n-1-k}(1-h) \right) \right). \tag{39}$$

Now, we note that

$$T_V^{n-1}(1-h) = \sum_{k=1}^{n-1} \frac{1}{2^k} T_V^{n-1-k}(1-h) \quad (n \rightarrow \infty), \tag{40}$$

so these terms cancel each other out in the limit and we are left with

$$D_V(h) = \frac{h}{2} + t_V(h). \tag{41}$$

If we let $n \rightarrow \infty$ in equation (32) then

$$\frac{t_M(h)}{2^n} \rightarrow 0 \quad n \rightarrow \infty \tag{42}$$

and hence we are left with the expression

$$D_M(h) = \frac{h}{2} + t_M(h). \tag{43}$$

We can see from equation (34) and equation (37) that $t_M(h) = t_V(h)$ when $h \in [0.5, 1]$ and hence the two diffusion coefficients are equal despite $M_h(x)$ being non-ergodic and $V_h(x)$ ergodic in this parameter range. The two equations (39) and (32) tell us that $D_M(h)$ and $D_V(h)$ converge at different rates and are only equal in the limit $n \rightarrow \infty$. We can explain this phenomenon by noting that the expression for the diffusion coefficient is only dependent on $t_M(h)$ or $t_V(h)$ and that these functions are only dependent on the branch of the map in $[0.5, 1]$. We interpret this phenomenon physically as the diffusion undergoing a dominating branch process, i.e. the diffusion coefficient is only dependent on the contribution of one branch of the map in the limit as $n \rightarrow \infty$. Hence we see identical diffusion coefficients despite the different microscopic dynamics.

We find a similar situation for $h \in [0, 0.5]$, where the lifted negative Bernoulli shift map and the lifted V map have the same diffusion coefficient. They have the branch in $[0, 0.5]$ in common in this parameter range and it is this which creates the dominating branch process. Hence we also observe identical diffusion coefficients between these two maps in this parameter range.

5. Conclusion

We have derived exact analytical expressions for the parameter dependent diffusion coefficients of four one-dimensional diffusive maps. This was achieved by using Taylor–Green–Kubo formulae and generalized Takagi functions. Under parameter variation we have observed both fractal and linear behaviour in the diffusion coefficients. The fractality was explained in terms of the topological instability of the maps under parameter variation and this was understood by analysing Markov partitions of the map. The linearity was explained in terms of the non-ergodicity of the maps in certain parameter ranges, which splits the phase space up into two ergodic components each with their own diffusion coefficient. These individual diffusion coefficients complement each other to create a linear diffusion coefficient. We also observed linear diffusion coefficients despite all the hallmarks of the dynamics for generating fractality being present. In this case we found that in the relevant parameter ranges, the ergodic maps have a set of branches in common with the non-ergodic maps which dominate the diffusion process in the long time limit, hence we observe identical diffusion coefficients. Based on the study of a variety of models, in previous literature it was conjectured that sufficiently low-dimensional deterministically chaotic dynamical systems generating transport on periodic lattices should typically exhibit irregular or fractal transport coefficients [3, 13, 14]. Typicality does not exclude that there exist specific counterexamples. Here we have identified a novel non-trivial mechanism leading to piecewise linearity, despite the maps fulfilling the above assumptions while even being topologically unstable and ergodic under parameter variation. This finding also contradicts the intuition that dynamical systems corresponding to linear diffusion coefficients are topologically stable.

So far this mechanism has only been confirmed for two piecewise linear maps whose microscopic symmetry is broken, which seems to be intimately related to the existence of a dominating branch. Future work may involve finding out under exactly which conditions we can manipulate the microscopic dynamics of such maps and still observe identical diffusion coefficients. We would also like to learn whether there exist any more physically realistic systems which display this dominating branch phenomenon. We could potentially apply the techniques used here to higher dimensional systems and see if we still obtain similar results. Also of interest is the consequences of introducing a bias into the system generating a current. It would be worthwhile to study whether analogous phenomena exist for this other transport property and whether they can be revealed by similar techniques.

Acknowledgments

The authors would like to thank Professor Gerhard Keller for helpful discussions about this work. They would like to dedicate this paper to the memory of Professor Shuichi Tasaki, a pioneer in the field of dynamical systems theory applied to nonequilibrium statistical mechanics.

References

- [1] Gaspard P 1998 *Chaos, Scattering and Statistical Mechanics* (Cambridge: Cambridge University Press)
- [2] Dorfman J R 1999 *An Introduction to Chaos in Nonequilibrium Statistical Mechanics* (Cambridge: Cambridge University Press)
- [3] Klages R 2007 *Microscopic Chaos, Fractals and Transport in Nonequilibrium Statistical Mechanics* (Singapore: World Scientific)
- [4] Geisel T and Nierwetberg J 1982 Onset of diffusion and universal scaling in chaotic systems *Phys. Rev. Lett.* **48** 7–10
- [5] Schell M, Fraser S and Kapral R 1982 Diffusive dynamics in systems with translational symmetry: a one-dimensional-map model *Phys. Rev. A* **26** 504–21
- [6] Fujisaka H and Grossmann S 1982 Chaos-induced diffusion in nonlinear discrete dynamics *Z. Phys. B–Condens. Matter* **48** 261–75
- [7] Klages R and Dorfman J R 1995 Simple maps with fractal diffusion coefficients *Phys. Rev. Lett.* **74** 387–90
- [8] Groeneveld J and Klages R 2002 Negative and nonlinear response in an exactly solved dynamical model of particle transport *J. Statist. Phys.* **109** 821–61
- [9] Gaspard P and Klages R 1998 Chaotic and fractal properties of deterministic diffusion–reaction processes *Chaos*. **8** 409–23
- [10] Cvitanović P, Artuso R, Mainieri R, Tanner G and Vattay G 2009 *Chaos: Classical and Quantum* (Copenhagen: Niels Bohr Institute) <http://chaosbook.org>
- [11] Korabel N and Klages R 2004 Fractality of deterministic diffusion in the nonhyperbolic climbing sine map *Physica D* **187** 66–88
- [12] Klages R, Barna I F and Matyas L 2004 Spiral modes in the diffusion of a single granular particle on a vibrating surface *Phys. Lett. A* **333** 79–84
- [13] Klages R 1996 *Deterministic Diffusion in One-Dimensional Chaotic Dynamical Systems* (Berlin: Wissenschaft and Technik)
- [14] Klages R and Dorfman J R 1999 Simple deterministic dynamical systems with fractal diffusion coefficients *Phys. Rev. E* **59** 5361–83
- [15] Dettmann C P and Morriss G P 1997 Stability ordering of cycle expansions *Phys. Rev. Lett.* **78** 4201–4
- [16] Cristadoro G 2006 Fractal diffusion coefficients from dynamical zeta functions *J. Phys. A: Math. Gen.* **39** L151–7
- [17] Klages R and Dorfman J R 1997 Dynamical crossover in deterministic diffusion *Phys. Rev. E* **55** R1247–50
- [18] Klages R and Klauss T 2003 Fractal dimensions of deterministic transport coefficients *J. Phys. A: Math. Gen.* **36** 5747–64
- [19] Petersen K 1983 *Ergodic Theory* (*Cambridge Studies in Advanced Mathematics* vol 2) (Cambridge: Cambridge University Press)
- [20] Knight G and Klages R 2010 Linear and fractal diffusion coefficients in a family of one dimensional chaotic maps, [arXiv:1007.3393](https://arxiv.org/abs/1007.3393)